Controlled deflection of cold atomic clouds and of Bose-Einstein condensates

Naceur Gaaloul, Laurence Pruvost, Mourad Telmini, Eric Charron

Controlled deflection of a cold atomic cloud

Naceur Gaaloul,[1,2] Laurence Pruvost,[3] Mourad Telmini,[2] and Eric Charron[1]

[1] *Laboratoire de Photophysique Moléculaire du CNRS, Université Paris-Sud, Bâtiment 210, 91405 Orsay Cedex, France.*

[2] *Laboratoire de Spectroscopie Atomique, Moléculaire et Applications, Département de Physique, Faculté des Sciences de Tunis, Université Tunis El Manar, 2092 Tunis, Tunisia.*

[3] *Laboratoire Aimé Cotton du CNRS, Université Paris-Sud, Bâtiment 505, 91405 Orsay Cedex, France.*

(Dated: September 17, 2007)

Abstract

We present a detailed, realistic proposal and analysis of the implementation of a cold atom deflector using time-dependent far off-resonance optical guides. An analytical model and numerical simulations are used to illustrate its characteristics. We show that it is possible to deflect almost entirely a cloud of ^{87}Rb falling in the gravity field with angles reaching up to 25 degrees, using for all relevant parameters values that are achieved with present technology. We discuss the limits of this proposed setup, and illustrate its strong robustness against non-adiabatic transitions.

PACS numbers: 03.75.Be, 32.80.Pj, 32.80.–t, 39.25.+k

I. INTRODUCTION

Optical and magnetic fields are extremely efficient tools used for the controlled manipulation of large ensembles of cold atoms [1, 2]. In the past fifteen years, cold matter waves have shown great possibilities in the context of linear atom optics, when phase-space densities are sufficiently low that the effect of collisions can be neglected. Dipole and radiation-pressure forces have for instance allowed the achievement of various optical manipulations such as atomic focusing, diffraction or interference [3, 4].

Many efforts have been recently devoted to the experimental implementation of atomic beam splitters with magnetic [5, 6, 7, 8] or optical [9, 10, 11] potentials. These different experimental investigations were accompanied by various theoretical studies [12, 13, 14, 15, 16]. These devices are obviously of clear interest for atom interferometry experiments. After the advent of Bose-Einstein condensation (BEC) in 1995 [17, 18], different setups were designed in order to split and recombine a BEC [19, 20, 21]. In this case, the experimental implementation is even more difficult since inter-atomic interactions due to high atomic densities in the wave-guides can sometimes not only induce the fragmentation of the BEC [22, 23], but also affect the overall coherence of the system [24].

In the present paper, we employ a semi-classical model derived recently for the description of the splitting dynamics of a cold atomic cloud [15] in order to show that a judicious modification of these devices can transform them into efficient coherent atom deflectors.

As illustrated in Fig. 1(a), we use for this demonstration a specific setup involving two crossing far off-resonant dipole guides. A similar setup was initially implemented experimentally in Orsay [9] in order to study the splitting of an atomic cloud. A large ensemble ($10^5 - 10^6$) of ^{87}Rb atoms is initially trapped and cooled in a magneto-optical trap (MOT) located around $z = 0$ in Fig. 1(a). The MOT is switched off at time $t = 0$, while a vertical far off-resonant laser beam, crossing the cloud close to its center, is switched on. A significant portion of the atoms, falling due to gravity, is captured and guided in this vertical wave-guide [9, 15]. When the center of the guided cloud reaches a given height $z = -h$, at time $t = t_c$, the vertical laser beam is switched off while a second oblique guide is switched on. This timing sequence is illustrated schematically in Fig. 1(b). The durations of the switching-on and -off are supposed to be much shorter than the typical time scale of the fall dynamics. In spite of the high velocities achieved in this vertical fall, we will show that a

good synchronization of this process allows for the implementation of an efficient deflector since the atomic cloud can be deviated from its initial trajectory up to a deflection angle of about 25 degrees with no significant atom loss.

The outline of the paper is as follows: in Sec. II we discuss the properties of ^{87}Rb atoms that are relevant for our analysis and describe our numerical model. We also give the values of typical laser parameters that realize this atom deflector. In Sec. III we give the results of our numerical investigations on its performance. We show that a high efficiency ($\geqslant 90\%$) can be achieved with large deflection angles. We also discuss the adiabaticity of the deflection process. Our conclusions are finally summarized in the last section.

II. THEORETICAL MODEL

During the guiding process and in the case of a large detuning, the atoms are subjected to a dipole force induced by the dipole potential

$$\mathcal{U}(\boldsymbol{r}) = \frac{\hbar\Gamma}{2}\,\frac{I(\boldsymbol{r})/I_s}{4\delta/\Gamma}\,, \tag{1}$$

where $\delta = \omega_L - \omega_0$ denotes the detuning between the laser angular frequency ω_L and the atomic transition frequency ω_0. I_s is the saturation intensity, and Γ the natural linewidth of the atomic transition [26].

In our numerical treatment, the atomic dynamics is restricted to the plane (x, z) defined by the two guides (see Fig. 1(a)). This implies a strong confinement in the y-direction. The transverse intensity distribution of the TEM_{00} vertical laser beam of power P_0 is approximated by the Gaussian-like form

$$\begin{aligned} &\text{if } |x| \leqslant \ell_0 : \quad I_0(x) \;=\; \frac{2P_0}{\pi w_0^2}\,\sin^2\left(\frac{\pi}{2}\,\frac{x-\ell_0}{\ell_0}\right)\,, \\ &\text{if } |x| > \ell_0 : \quad I_0(x) \;=\; 0\,, \end{aligned} \tag{2}$$

where the size ℓ_0 of the vertical guide is simply related to the laser waist w_0 by the relation

$$\ell_0 = w_0\sqrt{2\ln 2} \sim 1.18\, w_0\,. \tag{3}$$

This sinus-squared shape, which is often used in time-dependent calculations [25], is extremely close to the ideal Gaussian intensity distribution, except for the abscence of the extended wings of the true Gaussian shape which lengthen the calculations without any

noticeable contribution to the physical processes. With this sinus-squared convention, the guiding region ($|x| \leqslant \ell_0$) is also well defined. The trapping potentials associated with the vertical and oblique laser guides are thus expressed as

$$\mathcal{U}_0(x) \;=\; -U_0 \sin^2\left(\frac{\pi}{2}\,\frac{x-\ell_0}{\ell_0}\right) \quad \text{for } |x| \leqslant \ell_0 \tag{4a}$$

$$\mathcal{U}_1(x,z) \;=\; -U_1 \sin^2\left(\frac{\pi}{2}\,\frac{x'-\ell_1}{\ell_1}\right) \text{ for } |x'| \leqslant \ell_1 \tag{4b}$$

where x' denotes the rotated coordinate

$$x' = x\cos\gamma + (z+h)\sin\gamma\,. \tag{5}$$

Typical laser powers $P_0 \sim 5-30\,\mathrm{W}$ for a Nd:YAG laser operating at 1064 nm with laser waists of about $100-300\,\mu$m yield potential depths of about $5-250\,\mu$K. With these laser parameters, the ^{87}Rb transition to consider is the $\mathrm{D}_1:\ 5^2\mathrm{S}_{1/2} \rightarrow 5^2\mathrm{P}_{1/2}$, with a decay rate $\Gamma/2\pi \simeq 5.75\,\mathrm{MHz}$, a saturation intensity $I_s \simeq 4.5\,\mathrm{mW/cm^2}$ and a detuning $\delta/2\pi \simeq -95.4\,\mathrm{THz}$. With these conditions, the Rayleigh range $z_R = \pi w_0^2/\lambda$ is about 3 cm, thus allowing us to neglect the divergence of the beam on a length up to about 1 cm.

The guided atomic dynamics is followed by solving numerically the time-dependent Schrödinger equation for the atomic translational coordinates, taking into account the effect of the gravity field, and choosing realistic values for all laser parameters. We adopt a semi-classical approach where the z coordinate is described classically, following

$$t \leqslant t_c: \quad z_{cl}(t) \;=\; -\frac{1}{2}gt^2 \tag{6a}$$

$$t \geqslant t_c: \quad z_{cl}(t) \;=\; -\frac{1}{2}g\left(t_c + (t-tc)\cos\gamma\right)^2, \tag{6b}$$

where $t_c = (2h/g)^{1/2}$ is the time at which the atoms reach the crossing point (position $z = -h$). These equations of motion are obtained under the assumption of energy conservation for a classical particle which is perfectly deflected, and which therefore follows the paths blazed initially by the vertical beam and later on by the oblique guide. The other dimension x is treated at the quantum level, and this semi-classical approach was largely discussed and compared to the experimental study [9] in Ref. [15]. The two-dimensional time-independent guiding potentials (4) are thus replaced by the one-dimensional time-dependent potential

$$t \leqslant t_c: \quad \mathcal{U}(x,t) \;=\; \mathcal{U}_0(x) \tag{7a}$$

$$t \geqslant t_c: \quad \mathcal{U}(x,t) \;=\; \mathcal{U}_1(x, z_{cl}(t))\,, \tag{7b}$$

and the quantum dynamics is now summarized in the one-dimensional time-dependent Hamiltonian

$$\hat{\mathcal{H}}(x,t) = -\frac{\hbar^2}{2m}\frac{\partial^2}{\partial x^2} + \mathcal{U}(x,t)\,, \tag{8}$$

where m denotes the ^{87}Rb atomic mass. The time-dependent Schrödinger equation

$$i\hbar\frac{\partial}{\partial t}\varphi(x,t) = \hat{\mathcal{H}}(x,t)\;\varphi(x,t)\,, \tag{9}$$

is then solved using the numerical split operator technique of the short-time propagator [27], assuming that the atom is initially ($t = 0$) in a well defined eigenstate v, of energy E_v, of the potential (4a). At the end of the propagation, the final wave function $\varphi(x, t_f)$ is analyzed spatially, in order to extract the deflection efficiency η_D. An averaging procedure over the set of possible initial states finally allows to calculate the total deflection probability $\langle\eta_D\rangle$ of the entire atomic cloud (see Ref. [15] and Sec. III B for details).

III. NUMERICAL RESULTS

A. Case of a single initial state

In this study, the value of the position h of the crossing point between the two guides is the main parameter which controls the efficiency of the deflector. Indeed, for large values of h, the atoms reach the crossing point with a large kinetic energy $E_c = mgh$, and they will not be deflected if this energy exceeds by far the binding energy in the oblique guide ($E_c \gg U_1 - E_v$). More precisely, in order to predict the largest value of the height h allowing for atomic deflection, one should compare the kinetic energy gained by the atoms along the direction x' transverse to the oblique guide at the position $z = -h - \ell_1/\sin\gamma$ [see Fig. 1(a)] with the binding energy $U_1 - E_v$. One can effectively expect that the deflection will fail if

$$mg\left(h + \frac{\ell_1}{\sin\gamma}\right)\sin^2\gamma > U_1 - E_v\,. \tag{10}$$

In this expression, the $\sin^2\gamma$ factor originates from the fact that the transverse direction x' of the deflecting beam makes an angle γ with the fall direction z. The validity of this simple prediction is illustrated in Fig. 2, which represents the deflection probability η_D as a function of h [Fig. 2(a)] and of $w_1 = \ell_1/\sqrt{2\ln 2}$ [Fig. 2(b)], all other parameters being fixed. These probabilities are calculated numerically for a given initial state $v = 0$ (solid line with red

circles) or $v = 2094$ (solid line with green squares). The energy of this highly excited state is about halfway in the potential. In both graphs, the frontiers defined by the inequality (10) are indicated by vertical dashed arrows. By comparison with the "exact" value obtained from the solution of the time-dependent Schrödinger equation (9), one can notice that these frontiers correspond to a deflection probability of 50%. This energy criterion, which simply compares the atomic kinetic energy with the binding energy in the oblique guide, can thus be used safely to predict the efficiency of this setup.

One can also notice in Fig. 2(a) the surprising different variations of η_D with h for $v = 0$ and $v = 2094$. The very different behavior of these two vibrational levels comes from the fact that $v = 0$ is associated with a well localized atomic wavefunction, deeply bound in an almost harmonic potential, while $v = 2094$ is entirely delocalized over a large spatial range $|x| \leqslant \ell_0/2$, since its energy is about halfway in the potential ($E_v \simeq U_0/2$). As a consequence, $v = 0$ satisfies fully the conditions imposed by the Ehrenfest theorem [28] and its evolution can be described classically, while $v = 2094$ shows a quantum behavior. For $v = 0$, as soon as the inequality (10) is satisfied, the deflection probability falls to zero, in agreement with the usual dynamics of a classical particle. On the other hand, the stationnary state $v = 2094$ can be seen as a coherent superposition of incoming and outgoing wave packets characterized by rather broad kinetic energy distributions $\Delta E_c \sim U_0/2$. The packet moving in the $+x$ direction will be easily captured by the oblique guide, while the packet moving in the opposite direction easily avoids this wave guide. These two different dynamics are not much affected by the exact value of the falling height h, and this explains the very slow variation of η_D with h in Fig. 2(a) for $v = 2094$.

The variation of η_D with w_1 [see Fig. 2(b)] is also extremely different for $v = 0$ and $v = 2094$. The case $v = 0$ can again be interpreted classically : when w_1 increases, the possibility is open for the atoms to fall from a higher distance $d = (h+\ell_1/\sin\gamma)$, thus gaining a larger kinetic energy. This explains the decrease of η_D with w_1 for $v = 0$. This variation is just reversed in the case of $v = 2094$. Here, the initial wave function is characterized by a large typical size of about $\Delta x \sim \ell_0$. An efficient deflector can thus only be obtained if the size of the oblique wave guide remains of the order of, or is higher than, this typical size ℓ_0. Consequently, for $v = 2094$, when w_1 decreases below w_0, the deflection probability decreases, as seen in Fig. 2(b).

Finally, it is worth noting that, due to the $\sin^2\gamma$ factor in the inequality (10), it is possible

to induce an efficient deflection of atoms with relatively large kinetic energies using modest laser powers, as long as the angle γ remains small. For instance, in the case $v = 0$ shown in Fig. 2(a), an almost perfect deflection is obtained for $h = 8.5\,\mathrm{mm}$, even though the total kinetic energy of the atom reaches then about $E_c \sim 900\,\mu\mathrm{K}$, *i.e.* 30 times the depth of the oblique wave guide. A larger deflection angle could be achieved easily and with a very high efficiency by simply adding a succession of several deflection setups, each one inducing a small deflection of about 10 degrees.

Another important issue for the preservation of the coherence properties of an atomic cloud is the adiabaticity of the process. Previous theoretical studies have shown that similar beam splitter setups are able to conserve the coherence of the system even for a thermal distribution of atoms with an average energy far exceeding the level spacing of the transverse confinement [13]. This surprising behavior results from the fact that non-adiabatic transitions are induced by the time derivative operator d/dt which does not couple states of opposite parities, thus preventing nearest neighbor transitions [10]. In comparison, transitions to other states presenting the same parity as the initial state are also not favored since they involve larger energy differences [16].

As shown in Fig. 3, this robustness to non-adiabatic transitions is also present in our deflection scheme. This figure represents the atomic probability distributions $|\varphi(x, t_f)|^2$ calculated 7 mm below the crossing point $z = -h$ for the initial state $v = 0$, with $h = 2\,\mathrm{mm}$ [Fig. 3(a)], $h = 7\,\mathrm{mm}$ [Fig. 3(b)], and $h = 9\,\mathrm{mm}$ [Fig. 3(c)]. The vibrational distributions obtained in the oblique guide after deflection are also shown in the small insets of Fig. 3(a) and 3(b). Even though the vibrational spacing in the trap is only of the order of $\hbar\omega \sim 10\,\mathrm{nK}$, the initial state $v = 0$ is preserved at 99.1% for $h = 2\,\mathrm{mm}$, and at 50.3% for $h = 7\,\mathrm{mm}$. Indeed, in the first case, only $v = 2$ is slightly populated (0.1%), while the first five even vibrational levels are populated in the second case. It is only when the falling height h approaches the limit given by the inequality (10) that the population of the initial state $v = 0$ is almost entirely redistributed to higher excited states, as seen in the wave function shown Fig. 3(c).

B. Initial vibrational distribution

Realistically, an atomic cloud of typical size σ_0 and temperature T_0 can be described as a statistical mixture of trapped states, represented by the density matrix

$$\rho(\sigma_0, T_0) = \sum_v c_v(\sigma_0, T_0)\ |v\rangle\langle v|\,, \tag{11}$$

where the coefficients $c_v(\sigma_0, T_0)$ are involved functions of the cloud parameters σ_0 and T_0 and of the wave guide parameters U_0 and w_0 [15]. The calculation of the total deflection probability of the entire cloud therefore requires to average incoherently the deflection probability of each possible initial vibrational level v, taking into account the weight functions $c_v(\sigma_0, T_0)$. It is also worth noting that typical initial vibrational distributions $P(v) = |c_v(\sigma_0, T_0)|^2$ are relatively flat when $k_B T \sim U_0$, except for the lowest energy states which are usually more populated [15].

Fig. 4 shows the variation of the deflection efficiency with the initial vibrational level v for a series of different laser parameters. The transverse trapping potential (4a) associated with the vertical wave guide supports about 5000 trapped states when $U_0 = 30\,\mu$K and $w_0 = 100\,\mu$m. One can notice the general tendency of measuring a lower deflection probability when v increases, in perfect agreement with the variation expected from the energy criterion (10). As one could have naively guessed, increasing U_1 [Fig. 4(a)] or decreasing γ [Fig. 4(b)] has a similar effect, it increases the deflection probability of any initial state. In these figures, the vertical dashed arrows indicate the limits defined by the inequality (10), which are again in good agreement with the "exact" numerical values.

Finally, Fig. 5 represents the averaged deflection probability $\langle \eta_D \rangle$ as a function of the deflection angle γ and of the potential depth U_1 of the oblique laser guide, for a thermal input state of size $\sigma_0 = 0.15\,$mm and temperature $T_0 = 10\mu$K, with $h = 4\,$mm [Fig. 5(a)] and $h = 1\,$mm [Fig. 5(b)]. Realistic values have been chosen for all laser parameters, close to the one used in the experimental study [9], and the coefficients $c_v(\sigma_0, T_0)$ of Eq. (11) were calculated following Ref. [15]. One can notice a rapid decrease of $\langle \eta_D \rangle$ when U_1 decreases and when γ increases. However, an almost complete deflection (93.8%) is still observed in the case $h = 1\,$mm with $\gamma = 25\,$deg and $U_1 = 120\,\mu$K, even though the total kinetic energy of the atoms reaches then about $Ec \sim 100\,\mu$K at the crossing point, all trapped states being significantly populated initially. For $\gamma = 10\,$deg, the deflection efficiency reaches 99.8%. We

have also verified that decreasing the temperature of the initial cloud increases significantly the deflection efficiency since it suppresses the population of the highest trapped states, for which the deflection process is less efficient [see Fig. 4]. It is also worth noting that since the deflection process is less efficient for the highest trapped levels, it could also be used to selectively separate the lowest energy levels of the trap. We finally expect that, because it behaves very well for the lowest trapped states, this setup could prove useful with Bose-Einstein condensates [23].

IV. CONCLUSION

In summary, we have presented a detailed analysis of the implementation of an optical deflector for cold atomic clouds. Our analysis is quite close to the experimental conditions, and is clearly within the reach of current technology. We have shown how to create a high performance deflector using two crossing laser beams which are switched on and off in a synchronized way. We have found that a $10\,\mu$K cloud of ^{87}Rb can be deflected by 25 degrees with an efficiency of about 94%, and by 10 degrees with an efficiency exceeding 99%. A succession of such deflecting setups at this small angle could also be implemented in order to achieve larger deflection angles with high fidelities. We have shown that this device is robust against non-adiabatic transitions, an undesirable effect which could have led to heating processes. A high degree of control can therefore be achieved with such quantum systems, opening some possibilities for a range of applications.

Acknowledgments

We acknowledge HPC facilities of the IDRIS-CNRS supercomputer center (Project No. 08-51459) and E.C acknowledges partial financial support from CEA via the LRC-DSM Grant No. 05-33. E.C. and L.P. acknowledge financial support from PPF "Information Quantique", and L.P. acknowledges financial support from IFRAF (Institut Francilien de Recherche sur les Atomes Froids). Laboratoire de Photophysique Moléculaire and Laboratoire Aimé Cotton are associated to Université Paris-Sud.

REFERENCES

[1] C. S. Adams, M. Sigel, and J. Mlynek, *Phys. Rep.* **240**, 143 (1994).

[2] V. I. Balykin and V. S. Letokhov, *Atom Optics with Laser Light*, Vol. 18 of *Laser Science and Technology*, Harwood Academic, New York (1995).

[3] P. R. Berman, *Atom Interferometry* (Academic Press, New York, 1997).

[4] P. Meystre, *Atom Optics*, AIP Press Springer-Verlag, New York (2001).

[5] D. Müller, E. Cornell, M. Prevedelli, P. Schwindt, A. Zozulya, and D. Anderson, *Opt. Lett.* **25**, 1382 (2000).

[6] D. Cassettari, B. Hessmo, R. Folman, T. Maier, and J. Schmiedmayer, Phys. Rev. Lett. **85**, 5483 (2000).

[7] D. Müller, E. A. Cornell, M. Prevedelli, P. D. D. Schwindt, Y.-J. Wang, and D. Z. Anderson, Phys. Rev. A **63**, 041602 R (2001).

[8] P. Hommelhoff, W. Hänsel, T. Steinmetz, T. W. Hänsch, and J. Reichel, *New J. Phys.* **7**, 3 (2005).

[9] O. Houde, D. Kadio and L. Pruvost, Phys. Rev. Lett. **85**, 5543 (2000).

[10] W. Hänsel, J. Reichel, P. Hommelhoff, and T. W. Hänsch, Phys. Rev. Lett. **86**, 608 (2001).

[11] R. Dumke, T. Müther, M. Volk, W. Ertmer, and G. Birkl, Phys. Rev. Lett. **89**, 220402 (2002).

[12] J. A. Stickney and A. A. Zozulya, Phys. Rev. A **68**, 013611 (2003).

[13] H. Kreutzmann, U. V. Poulsen, M. Lewenstein, R. Dumke, W. Ertmer, G. Birkl, and A. Sanpera, Phys. Rev. Lett. **92**, 163201 (2004).

[14] D. C. E. Bortolotti and J. L. Bohn, Phys. Rev. A **69**, 033607 (2004).

[15] N. Gaaloul, A. Suzor-Weiner, L. Pruvost, M. Telmini, and E. Charron, Phys. Rev. A **74**, 023620 (2006).

[16] M. Zhang, P. Zhang, M. S. Chapman, and L. You, Phys. Rev. Lett. **97**, 070403 (2006).

[17] M. H. Anderson, J. R. Ensher, M. R. Matthews, C. E. Wieman, and E. A. Cornell *Science* **269** 198 (1995).

[18] K. B. Davis, M. O. Mewes, M. R. Andrews, N. J. van Druten, D. S. Durfee, D. M. Kurn, and W. Ketterle, Phys. Rev. Lett. **75**, 3969 (1995).

[19] Y. Shin, M. Saba, T. A. Pasquini, W. Ketterle, D. E. Pritchard, and A. E. Leanhardt, Phys. Rev. Lett. **92**, 050405 (2004).

[20] Y. J. Wang, D. Z. Anderson, V. M. Bright, E. A. Cornell, Q. Diot, T. Kishimoto, M. Prentiss, R. A. Saravanan, S. R. Segal, and S. Wu, Phys. Rev. Lett. **94**, 090405 (2005).

[21] T. Schumm, S. Hofferberth, L. M. Andersson, S. Wildermuth, S. Groth, I. Bar-Joseph, J. Schmiedmayer, and P. Krüger, *Nat. Phys.* **1**, 57 (2005).

[22] J. A. Stickney and A. A. Zozulya, Phys. Rev. A **66**, 053601 (2002).

[23] N. Gaaloul, A. Jaouadi, M. Telmini, L. Pruvost, and Eric Charron, *AIP Conf. Proc.*, **935**, 10 (2007).

[24] S. Chen and R. Egger, Phys. Rev. A **68**, 063605 (2003).

[25] A. Giusti-Suzor, F. Mies, L. Di-Mauro, E. Charron, and B. Yang, Topical Review of *J. Phys. B: At. Mol. Opt. Phys.*, **28**, 309, (1995).

[26] W. D. Phillips, in *Fundamental Systems in Quantum Optics*, Proceedings of the Les Houches Summer School, (North-Holland, Amsterdam, 1992).

[27] M. J. Feit, J. A. Fleck and A. Steiger, *J. Comput. Phys.* **47**, 412 (1982).

[28] P. Ehrenfest, *Z. Phys.* **45**, 455 (1927).

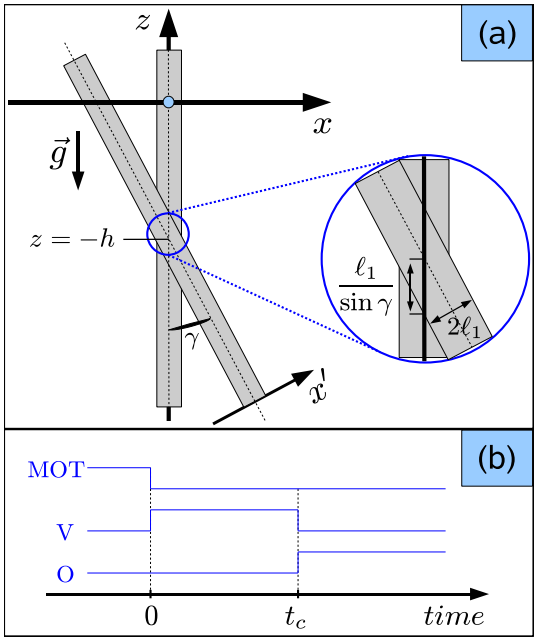

FIG. 1: (Color online) (a) Schematic representation of the proposed optical deflector for cold atoms. The right inset is a magnification of the crossing region. The vertical position of the crossing point is $z = -h$, and the total transverse width of the oblique guide is equal to $2\ell_1$. (b) Timing of the magnetic and optical trap (MOT) and of the vertical (V) and oblique (O) guides used in this setup. t_c corresponds to the date at which the Rb atoms reach the crossing height $z = -h$.

FIGURE 1

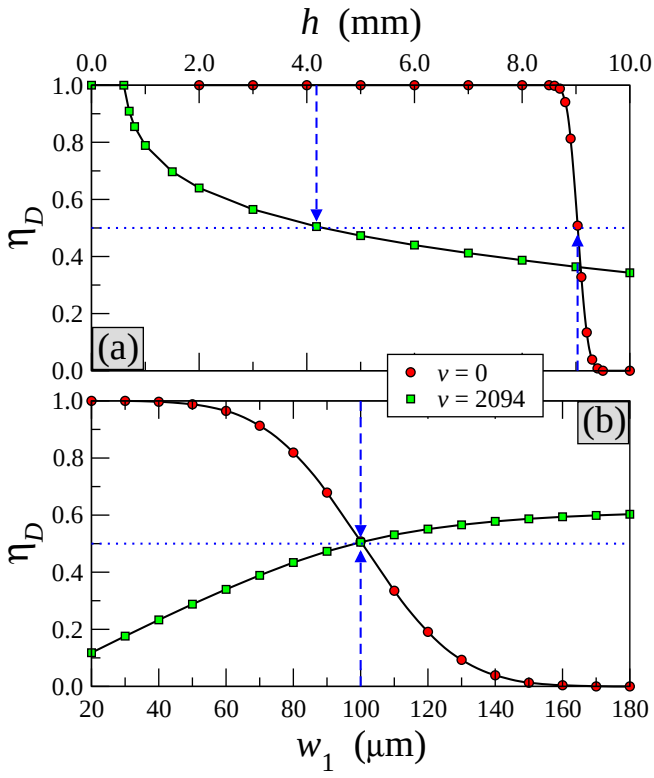

FIG. 2: (Color online) Deflection probability η_D as a function (a) of the falling distance h [see Fig. 1] and (b) of the waist w_1 of the oblique laser beam. These results are for a single initial state : $v = 0$ (solid line with red circles) or $v = 2094$ (solid line with green squares). In both graphs, the dashed blue arrows mark the position at which a deflection efficiency of 50% is expected according to inequality (10). The laser parameters have been chosen such that $U_0 = U_1 = 30\,\mu$K, and $w_0 = 100\,\mu$m. In graph (a) the oblique laser waist is $w_1 = 100\,\mu$m and in graph (b) the height h is equal to 9.03 mm for $v = 0$ and to 4.18 mm for $v = 2094$.

FIGURE 2

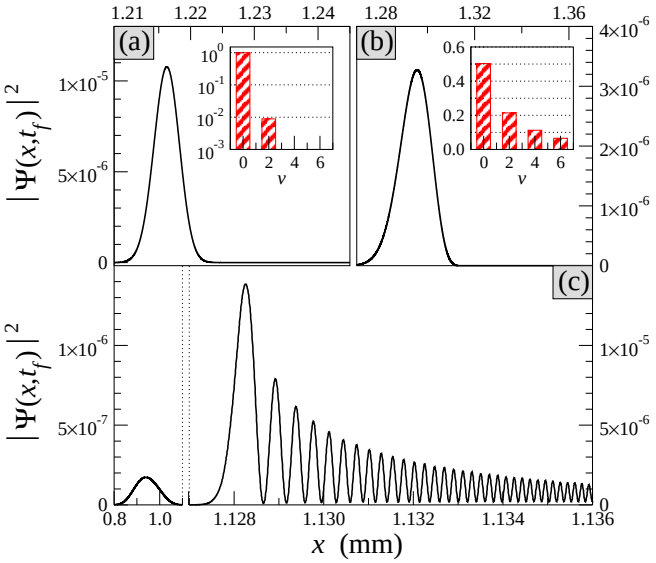

FIG. 3: Atomic probability distributions $|\varphi(x,t_f)|^2$ as a function of the transverse coordinate x at the end of the propagation, for (a) h =2 mm, (b) h =7 mm and (c) h = 9 mm. The laser parameters are identical to the one of Fig. 1, with $v = 0$ and $w_1 = 100\,\mu$m. Note that, for the sake of clarity, the horizontal axis has been broken in panel (c). The small insets in panels (a) and (b) represent the vibrational distributions in the oblique guide at the end of the propagation.

FIGURE 3

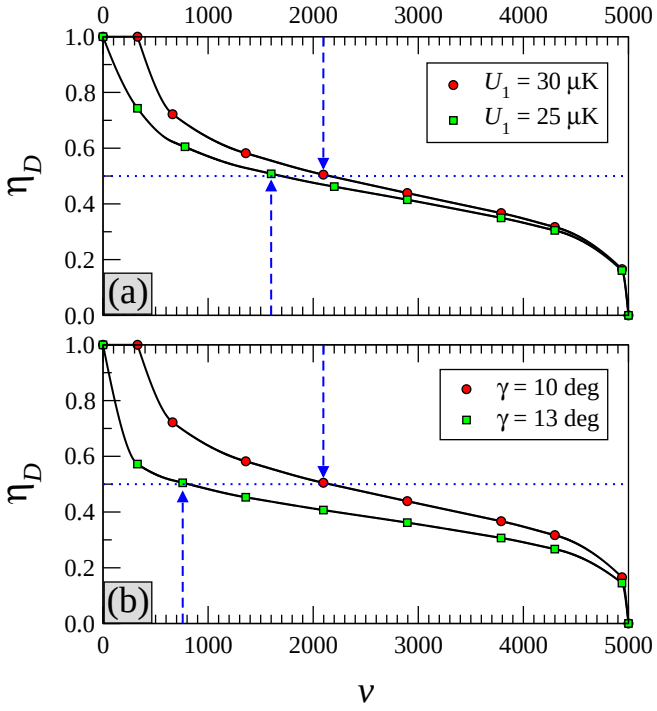

FIG. 4: (Color online)(Color online) Deflection probability η_D as a function of the initial vibrational level v. (a) The deflection angle is equal to $\gamma = 10\,\text{deg}$, and the solid line with red circles stands for $U_1 = 30\,\mu\text{K}$ while the solid line with green squares is for $U_1 = 25\,\mu\text{K}$. (b) The depth of the oblique wave guide is equal to $U_1 = 30\,\mu\text{K}$, and the solid line with red circles stands for $\gamma = 10\,\text{deg}$ while the solid line with green squares is for $\gamma = 13\,\text{deg}$. In both graphs, the dashed blue arrows mark, in each case, the positions at which a deflection efficiency of 50% is expected according to the inequality (10). The falling height is $h = 4\,\text{mm}$ and the oblique laser waist is equal to $w_1 = 100\,\mu\text{m}$. All other laser parameters are identical to the one of Fig. 1.

FIGURE 4

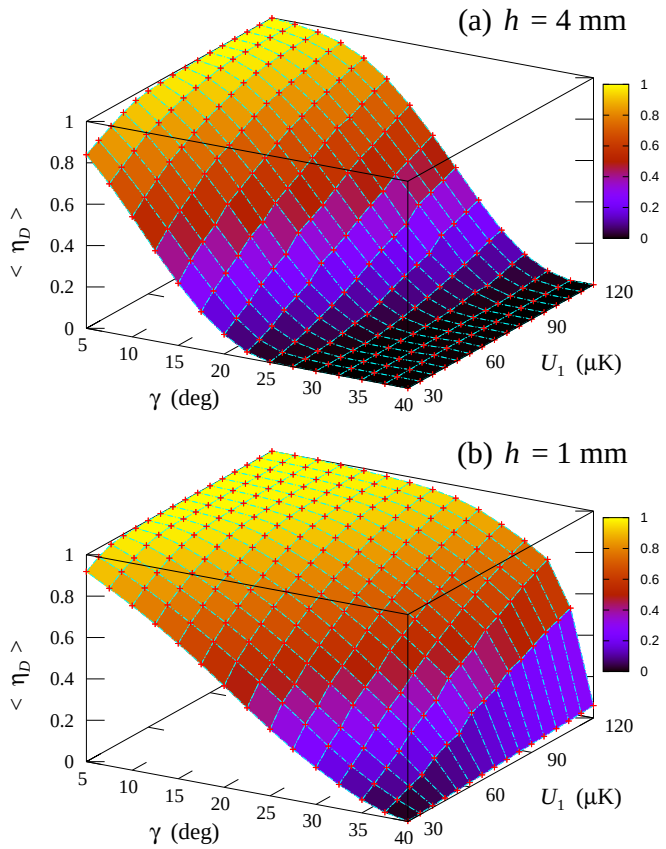

FIG. 5: (Color online) Total deflection probability $\langle \eta_D \rangle$ of an atomic cloud of ^{87}Rb of size $\sigma_0 = 0.15\,\mathrm{mm}$ at temperature $T_0 = 10\,\mu\mathrm{K}$. The laser parameters have been chosen such that $U_0 = 30\,\mu\mathrm{K}$, $w_0 = 200\,\mu\mathrm{m}$, $w_1 = 158\,\mu\mathrm{m}$, and $h = 4\,\mathrm{mm}$ (a) or $h = 1\,\mathrm{mm}$ (b).

FIGURE 5